Journal of Molecular Catalysis A: Chemical 349 (2011) 48–54

Contents lists available at SciVerse ScienceDirect

Journal of Molecular Catalysis A: Chemical

journal homepage: www.elsevier.com/locate/molcata

Catalytic combustion of hydrogen over $La_{1-x}Sr_xCoO_{3-\delta}$ + Co_3O_4 and $LaMn_{1-x}Cu_xO_{3+\delta}$ under simulated MCFC anode off-gas conditions

Hee-Jun Eom [a], Jun Ho Jang [a], Dae-Won Lee [b,*], Seongmin Kim [a], Kwan-Young Lee [a,c,**]

[a] Department of Chemical and Biological Engineering, Korea University, 5-1, Anam-dong, Sungbuk-ku, Seoul 136-701, South Korea
[b] Research Institute of Clean Chemical Engineering Systems, Korea University, 5-1, Anam-dong, Sungbuk-ku, Seoul 136-701, South Korea
[c] Green School, Korea University, 5-1, Anam-dong, Sungbuk-ku, Seoul 136-701, South Korea

ARTICLE INFO

Article history:
Received 6 May 2011
Received in revised form 3 August 2011
Accepted 19 August 2011
Available online 26 August 2011

Keywords:
Perovskite
$La_{1-x}Sr_xCoO_{3-\delta}$
$LaMn_{1-x}Cu_xO_{3+\delta}$
Hydrogen combustion
O_2-TPD
TPR

ABSTRACT

The activities of two perovskite catalysts, $LaMn_{1-x}Cu_xO_{3+\delta}$ ($0 \le x \le 1$) and $La_{1-x}Sr_xCoO_{3-\delta}$ ($0 \le x \le 1$), were tested for the catalytic combustion of hydrogen under simulated molten carbonate fuel cell (MCFC) anode off-gas conditions. The catalysts were prepared using the sol–gel citrate (SGC) method and were characterized by X-ray diffraction (XRD), Brunauer–Emmett–Teller (BET) analysis, oxygen temperature-programmed desorption (O_2-TPD), and temperature-programmed reduction (TPR) in order to discriminate the major properties governing the activities of the catalysts. The activity of $LaMn_{1-x}Cu_xO_{3+\delta}$ was the highest at $x = 0.4$, at which the reducibility of B-site cations and mobility of active oxygen were the most prominent. The activity of $La_{1-x}Sr_xCoO_{3-\delta}$ was strongly related to the amount of oxygen vacancies, and the by-produced Co_3O_4 had a positive effect, which was the reason why the catalyst at $x = 0.6$ (a mixture of $La_{1-x}Sr_xCoO_{3-\delta}$ + Co_3O_4) was comparatively active to those at $x = 0.2$ and 0.4.

1. Introduction

With the growing prospect of hydrogen as a sustainable energy infrastructure in the near future, much research and development has focused on the commercialization of technologies relating to the production, utilization, and storage of hydrogen. Current commercial routes for producing hydrogen are based on the catalytic steam reforming of hydrocarbons. The majority of hydrogen sources are fossil fuels such as oil, coal, and natural gas. Recently, with the goal of strengthening sustainability, researchers have been intensively examining the use of biomasses such as kraft lignin, sawdust, and algae, as a source of hydrogen [1,2]. For the utilization of hydrogen, fuel cells are the optimal choice for both energy transportation and storage applications. As fuel cell technologies approach commercialization, new technical requirements have appeared, especially in the area of Balance of Fuel Cell Power Plants (BOP) systems. One such requirement is the utilization of leftover hydrogen in electrode off-gases. A feasible plan would be the use of off-gases as a fuel for a catalytic combustor, which assists in the heating of electrode stacks [3]. For the catalytic combustion of hydrogen, a precious metal (Pt or Pd) catalyst must be chosen preferentially if the conversion rate of hydrogen is the only consideration. However, such precious metal catalysts frequently suffer losses in activity at elevated temperatures through thermal agglomeration or volatilization of active metals [4]. Moreover, fuel cell system developers generally think it is undesirable to use such expensive catalysts in BOP system. Therefore, a thermally durable and less expensive catalyst is needed for the catalytic combustor in BOP system [5]. In this study, we chose perovskite catalysts ($LaMn_{1-x}Cu_xO_{3+\delta}$ and $La_{1-x}Sr_xCoO_{3-\delta}$) as candidate catalysts for such an application.

Perovskites are $A^{+3}B^{+3}O_3$ type oxides (A = usually La when used as a catalyst; B = Mn, Co, Cr, Fe, Ni, etc.) that are utilized as catalysts in various industrial reactions, including oxidation of hydrocarbons, carbon monoxide and carbon particulates [6–8]. These perovskite catalysts offer good thermal stability, as the lattices are crystallized at high temperature, usually over 750 °C [9]. Their high oxidation activity, thermal durability and cheap material cost have made them widely applicable in catalytic combustion. Unlike other solid catalysts, a high specific surface area is not strictly required for a perovskite catalyst, as catalytic activity is mostly dependent on the redox behavior of B-site cations located in the bulk, as well as on the surface [7,10]. Along with the redox property

* Corresponding author at: Research Institute of Clean Chemical Engineering Systems, Korea University, 5-1, Anam-dong, Sungbuk-ku, Seoul 136-701, South Korea. Tel.: +82 2 3290 3727; fax: +82 2 926 6102.
** Corresponding author at: Green School, Korea University, 5-1, Anam-dong, Sungbuk-ku, Seoul 136-701, South Korea. Tel.: +82 2 3290 3727; fax: +82 2 926 6102.
E-mail addresses: stayheavy@korea.ac.kr (D.-W. Lee), kylee@korea.ac.kr (K.-Y. Lee).

1381-1169/$ – see front matter © 2011 Elsevier B.V. All rights reserved.
doi:10.1016/j.molcata.2011.08.017

of B-site cations, structural defects such as cation and oxygen deficiencies also play important roles in the mechanism of catalysis [7]. These redox properties and structural defects are basically dependent on the kinds of A- and B-site elements, and change dynamically upon substitution of the elements with a metal ion of smaller valence state (+2) [6,7,10,11].

Among the numerous kinds of substituted perovskites, $LaMn_{1-x}Cu(+2)_xO_{3+\delta}$ and $La_{1-x}Sr(+2)_xCoO_{3-\delta}$ are frequently studied as oxidation catalysts due to their high activities and thermal stabilities in the oxidation of methane [12–14], propane [15], volatile organic compounds (VOC) [16], hydrogen [17,18], hydrogen sulfide [19] and carbon monoxide [15,17,20–22].

The $LaMnO_{3+\delta}$ catalyst is well known to have oxygen-excess nonstoichiometry ($3+\delta$) caused by the cationic vacancies and Mn^{4+} ions that are formed to mitigate the static Jahn–Teller distortion of Mn^{3+} ions in the perovskite lattice [15]. The partial substitution of Cu^{2+} for Mn ions changes the numbers of cationic vacancies and Mn^{4+} ions, consequently influencing the oxidative activity of the catalyst [14,15]. For $La_{1-x}Sr_xCoO_{3-\delta}$ catalyst, Sr^{2+} substitution increments the numbers of oxygen vacancies and/or Co^{4+} ions as the catalyst neutralizes the charge caused by the substitution [15,17,20,23]. The numbers of oxygen vacancies and Co^{4+} ions are closely related to the catalytic activities of the substituted perovskite catalysts [15,17,20,23].

In this study, the activities of $LaMn_{1-x}Cu_xO_{3+\delta}$ and $La_{1-x}Sr_xCoO_{3-\delta}$ were examined for the catalytic combustion of hydrogen under the simulated conditions of a molten carbonate fuel cell (MCFC) anode off-gas. The MCFC anode off-gas contains H_2O and CO_2, both of which are known to influence catalysis over perovskite [24]. The activity of perovskite catalysts for hydrogen oxidation has been studied in the past [17,18], but as far as authors know, it has not yet been tested under a MCFC anode off-gas conditions. The study focused on determining the key catalytic properties of the two perovskites that regulate hydrogen combustion under MCFC anode off-gas conditions. For this, we used X-ray diffraction (XRD), Brunauer–Emmett–Teller (BET) analysis, oxygen temperature-programmed desorption (O_2-TPD) and temperature-programmed reduction (TPR).

2. Experimental

2.1. Preparation of catalysts

Perovskite catalysts were prepared by the sol–gel citrate (SGC) method [1]. $La(NO_3)_3{\cdot}xH_2O$ (Aldrich, +99.9%), $Mn(NO_3)_2{\cdot}4H_2O$ (Aldrich, +99.2%), $Cu(NO_3)_2{\cdot}2.5H_2O$ (Aldrich, +98%), $Fe(NO_3)_3{\cdot}9H_2O$ (Aldrich, +98%), $Co(NO_3)_2{\cdot}6H_2O$ (Junsei Chemical, +97%) and $Sr(NO_3)_2$ (Aldrich, +99%) were used as precursors. The stoichiometric quantities of corresponding nitrates were dissolved in distilled water. The total molar concentration of nitrates was fixed at 0.1 mol/L. Citric acid (Aldrich, +99.5%) was added in 10 mol% excess over the stoichiometric molar quantity of dissolved metals. The resulting solution was stirred for 1 h and then evaporated in a rotary evaporator (165 °C) under reduced pressure until a viscous gel was obtained. The gel was dried overnight at 70 °C. The spongy material was finely crushed and calcined at 700 °C for 5 h. Since a nitrate–citrate mixture easily combusts in a sol–gel state, the temperature control and quantification of precursors were carried out in a cautious manner.

2.2. Characterization of catalysts

The specific surface area of the catalysts was measured by the BET method on an ASAP 2010 (Micromeritics) apparatus. The nitrogen adsorption–desorption isotherms were measured at −196 °C using 200 mg of sample. Before measurement, the sample was degassed at 250 °C and 4 mm Hg for 12 h. XRD patterns of the catalysts were obtained at room temperature using an X-ray diffractometer, D/MAX-2500 V/PC (Rigaku) operated with Ni-filtered Cu-Kα radiation (λ = 0.15418 nm) at 40 kV and 150 mA. The crystallite size of the perovskite phase was determined through Scherrer analysis applied to the [1 1 0] diffraction peak ($2\theta \fallingdotseq 32.5°$ for $LaMn_{1-x}Cu_xO_{3+\delta}$ and 32.9° for $La_{1-x}Sr_xCoO_{3-\delta}$). O_2-TPD and TPR analyses were performed on a BELCAT-M-77 instrument (BEL Japan Inc.). The detailed procedure of the O_2-TPD experiments was performed as follows: The catalyst (100 mg) was enclosed in a quartz tube and heated up to 700 °C under an O_2 flow (40 mL/min). The temperature was maintained at 700 °C for 1 h and then cooled down to room temperature under the same oxygen flow rate. Next, helium was fed to the catalyst at a flow rate of 35 mL/min, which was maintained for 1 h at room temperature to purge out excess oxygen on the catalyst surface. Finally, the catalyst was heated to 950 °C at a heating rate of 10 °C/min under a helium flow of 35 mL/min. The desorbed oxygen was measured by the TCD. TPR experiments were carried out after the same pretreatment steps adopted for the O_2-TPD. Then, the catalyst was heated to 1050 °C at a heating rate of 10 °C/min under a flow (35 mL/min) of 5% H_2/N_2 balance gas. The peaks in the O_2-TPD and TPR profiles were quantitatively estimated based on the calibration curves that were obtained by injecting oxygen (hydrogen) pulses of known volume in a helium (nitrogen) background flow. The calibrations were confirmed through probe TPR/O_2-TPD tests using commercial CuO powder (Aldrich, +99.995%). The amount of α-oxygen in the catalyst was obtained by quantification of the O_2-TPD peak that appeared at temperatures less than 500 °C. The oxygen non-stoichiometry (δ) of the catalyst was calculated by subtracting the 'theoretical value' from the 'actual value' for the oxygen stoichiometry. The theoretical oxygen stoichiometry was calculated based on the principle of electroneutrality. The 'actual' oxygen stoichiometry was estimated from the amount of removed oxygen ('Total O-removed') during the TPR run.

2.3. Catalytic activity tests

Catalytic activities were measured using a flow-type, packed-bed reactor under simulated MCFC anode off-gas conditions as follows: 3.3 vol% H_2, 10.7 vol% O_2, 16.5 vol% CO_2, 13.0 vol% H_2O, and balance N_2. The composition was based on the actual anode off-gas measured from an MCFC demo plant operated under steady state in Korea. The total gas flow rate was 300 mL/min. The catalysts were sieved, and powders sized 75–100 μm were used in the tests. One hundred milligrams of catalyst was packed in the middle of a tubular quartz reactor with quartz wool supporting the packed layer. The activity tests were performed in the temperature range of 200–500 °C (stepwise at intervals of 50 °C). Water was removed from the product gas by a cold trap, and the composition of the dehumidified gas was analyzed by gas chromatography (Young-lin) with a packed column (Porapak-Q, Alltech) and the TCD.

3. Results and discussion

3.1. Characterization of catalysts

3.1.1. XRD and BET

The XRD results of the prepared catalysts are presented in Fig. 1 ($LaMn_{1-x}Cu_xO_{3+\delta}$) and 2 ($La_{1-x}Sr_xCoO_{3-\delta}$). $LaMn_{1-x}Cu_xO_{3+\delta}$ (x = 0–0.8) (Fig. 1) exhibited a single-phase, perovskite-type structure (rhombohedral or cubic, Table 1) in accordance with the JCPDS database of $LaMnO_{3+\delta}$ (PDF #32-0484 and 75-0440). The presence of CuO was detected at x = 0–0.8, but the amount was negligibly

Table 1
Compositional and dimensional structure of $La_{1-x}Sr_xCoO_{3-\delta}$ and $LaMn_{1-x}Cu_xO_{3+\delta}$.

Catalyst	Structure[a]	Specific surface area ($m^2\ g^{-1}$)	Crystallite size of perovskite[b] (nm)	α-Oxygen [from O_2-TPD] (10^{-3} mol-O_2/g-cat.)	Total O-removed [from TPR] (10^{-3} mol-O/g-cat.)	Non-stoichiometry of oxygen (δ)
$LaCoO_{3-\delta}$	P	5.2	29.8	0.0419	5.4618	0.16
$La_{0.8}Sr_{0.2}CoO_{3-\delta}$	P	10.8	23.6	0.1486	6.4797	0.08
$La_{0.6}Sr_{0.4}CoO_{3-\delta}$	P + Co_3O_4 + $SrCO_3$	13.8	18.6	0.1128	7.2483	n.a.[c]
$La_{0.4}Sr_{0.6}CoO_{3-\delta}$	P + Co_3O_4 + $SrCO_3$	9.6	16.1	0.1521	7.4852	n.a.[c]
$La_{0.2}Sr_{0.8}CoO_{3-\delta}$	P + Co_3O_4 + $SrCO_3$	7.5	36.6	0.1332	7.9539	n.a.[c]
$SrCoO_{3-\delta}$	P + Co_3O_4 + $SrCO_3$	4.4	37.3	0.1561	8.2172	n.a.[c]
$LaMnO_{3+\delta}$	P (cubic)	39.3	14.4	0.0999	2.8856	0.20
$LaMn_{0.8}Cu_{0.2}O_{3+\delta}$	P (rhombohedral)	24.4	17.6	0.0775	3.2128	0.08
$LaMn_{0.6}Cu_{0.4}O_{3+\delta}$	P (cubic)	12.3	23.8	0.1098	3.8679	0.04
$LaMn_{0.4}Cu_{0.6}O_{3+\delta}$	P (cubic)	16.4	18.0	0.1850	4.1476	−0.08
$LaMn_{0.2}Cu_{0.8}O_{3+\delta}$	P (cubic)	13.7	18.3	0.2838	4.2239	−0.25
$La_2CuO_{4+\delta}$	A_2BO_4 type + CuO	8.0	39.1	0.1115	4.3261	n.a.[c]

[a] P: perovskite.
[b] The crystallite sizes were estimated with the Scherrer equation for [1 1 0] diffraction peaks.
[c] The values were 'not available' because the samples were not pure perovskites.

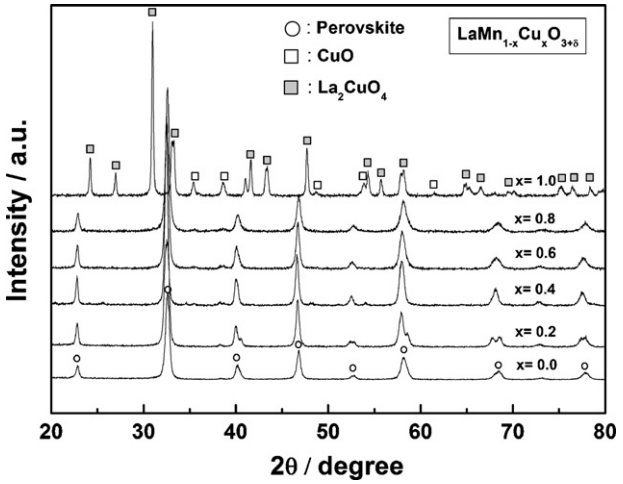

Fig. 1. XRD patterns of $LaMn_{1-x}Cu_xO_{3+\delta}$ ($0 \le x \le 1$).

small. On the contrary, the XRD results of $LaMn_{1-x}Cu_xO_{3+\delta}$ at $x = 1.0$ present the A_2BO_4-type perovskite structure (La_2CuO_4),containing a fair amount of by-produced CuO. $La_{1-x}Sr_xCoO_{3-\delta}$ (Fig. 2) exhibited a single-phase perovskite structure ($LaCoO_3$ at PDF #25-1060) at a degree of Sr substitution of $x = 0$ and 0.2. However, when x exceeded 0.2, by-produced phases such as $SrCO_3$ and Co_3O_4 appeared along with the perovskite oxide [25].

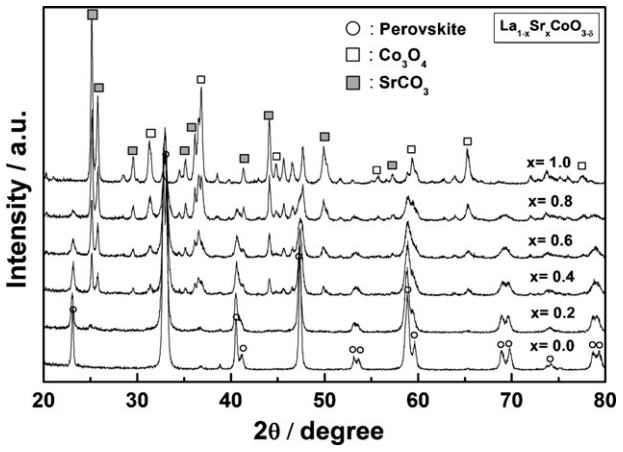

Fig. 2. XRD patterns of $La_{1-x}Sr_xCoO_{3-\delta}$ ($0 \le x \le 1$).

Regarding the specific surface area of the catalysts, Fig. 3 shows that the area of $LaMn_{1-x}Cu_xO_{3+\delta}$ decreased with increasing Cu substitution (x). The specific surface area decreased from 39.3 $m^2\ g^{-1}$ (for $x = 0$, $LaMnO_{3+\delta}$) to 13.7 $m^2\ g^{-1}$ (for $x = 0.8$, $LaMn_{0.2}Cu_{0.8}O_{3+\delta}$) as x was increased. The specific surface area of $La_{1-x}Sr_xCoO_{3-\delta}$ reached its highest value (13.8 $m^2\ g^{-1}$) at $x = 0.4$ and decreased monotonously with further increment of x. Table 1 lists the specific surface areas, crystallite sizes and oxygen non-stoichiometries of the prepared perovskites.

3.1.2. O_2-TPD and TPR

The oxidative activities of perovskite catalysts are frequently attributed to the intrinsic active oxygen species that are sourced from surface defects or bulk lattices [3,4]. The O_2-TPD tests were performed to investigate the active oxygen species of the prepared perovskites. The results are presented in Fig. 4 ($LaMn_{1-x}Cu_xO_{3+\delta}$) and 5 ($La_{1-x}Sr_xCoO_{3-\delta}$). In both perovskite catalysts, the desorbed oxygen species could be classified into two categories according to their origins [10,15,17,19,22,26]: The broad plateau-like peaks appearing below 600 °C corresponded to α-oxygen that originated from the oxygen vacancies on the suprafacial region. The sharp peaks appearing above 600–850 °C corresponded to β-oxygen that was desorbed through the reduction of B-site metal cations in the perovskite lattice.

For $LaMn_{1-x}Cu_xO_{3+\delta}$, the amount of α-oxygen generally increased as the degree of Cu substitution (x) increased. The amount

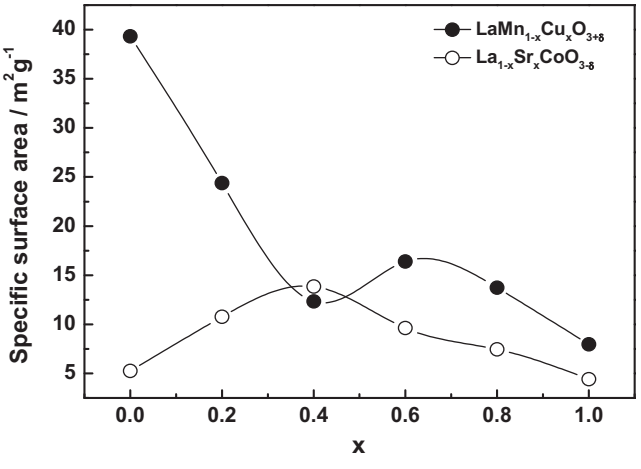

Fig. 3. Specific surface areas of $LaMn_{1-x}Cu_xO_{3+\delta}$ and $La_{1-x}Sr_xCoO_{3-\delta}$ ($0 \le x \le 1$).

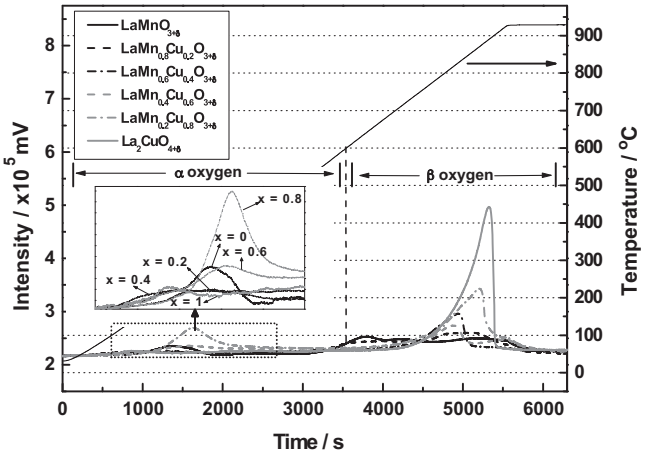

Fig. 4. O_2-TPD profiles for $LaMn_{1-x}Cu_xO_{3+\delta}$ ($0 \le x \le 1$).

of α-oxygen from the catalysts is listed in Table 1. The increase in α-oxygen was especially prominent at $x = 0.6$ ($LaMn_{0.4}Cu_{0.6}O_{3+\delta}$) and 0.8 ($LaMn_{0.2}Cu_{0.8}O_{3+\delta}$) where the amounts of α-oxygen (0.1850 and 0.2838×10^{-3} mol-O_2/g-cat, respectively) were approximately twice those of the single B-atom perovskites, $LaMnO_{3+\delta}$ and $La_2CuO_{4+\delta}$ (0.0999 and 0.1115×10^{-3} mol-O_2/g-cat, respectively). Lisi et al. reported, regarding the β-oxygen from $LaMn_{1-x}Cu_xO_{3+\delta}$, that the release of β-oxygen is prominent when the cationic vacancies (in La and Mn) remain in the lattice, which falls into the degree of Cu substitution (x) less than 0.4 [14]. However, in our TPD tests, β-oxygen desorption was still observed although x was over 0.4 and even became much larger at $x = 0.8$ and 1.0,with broadening of the desorption peak into higher temperature region (850–900 °C). This implies the presence of β-oxygen sources other than the cationic vacancy. Zhua et al. had observed a similar high-temperature peak of β-oxygen desorption from $La_2CuO_{4+\delta}$ [27].

In the case of $La_{1-x}Sr_xCoO_{3-\delta}$ (Fig. 5), both α- and β-oxygen desorptions were generally promoted with increasing Sr substitution (x). The sources of α- and β-oxygen in $La_{1-x}Sr_xCoO_{3-\delta}$ have been explained well in the literature [27]. The α desorption from $La_{1-x}Sr_xCoO_{3-\delta}$ is ascribed to oxygen embedded in the oxygen vacancies generated by the substitution of Sr^{2+}, and corresponds well in quantity to the nominal amount of Co^{4+} ions. The β-oxygen is ascribed to the lattice oxygen from the bulk perovskite phase, which corresponds with the $Co^{3+} \rightarrow Co^{2+}$ reduction (and $Co^{4+} \rightarrow Co^{3+}$reductionfor the samples with high Sr content). In our O_2-TPD results, an increase in β-oxygen capacity was noticeable upon substitution of Sr^{2+}, whereas the promotion of α-oxygen desorption was comparatively small. However, the quantitative comparison of α-oxygen among the samples was not meaningful, since some samples were not 100% perovskite and contained a fair amount of by-products ($SrCO_3$ and Co_3O_4). As the degree of Sr substitution (x) exceeded 0.4, the β-oxygen peak became bimodal with appearance of a high-temperature, structural collapse (or total reduction of B-site cation) peak. For the samples containing by-products ($x \ge 0.4$), the decomposition peak of Co_3O_4 was expected to overlap the β-oxygen signals over 900 °C. On the contrary, overlap of signals from $SrCO_3$ was not expected, since its decomposition occurs over 1290 °C.

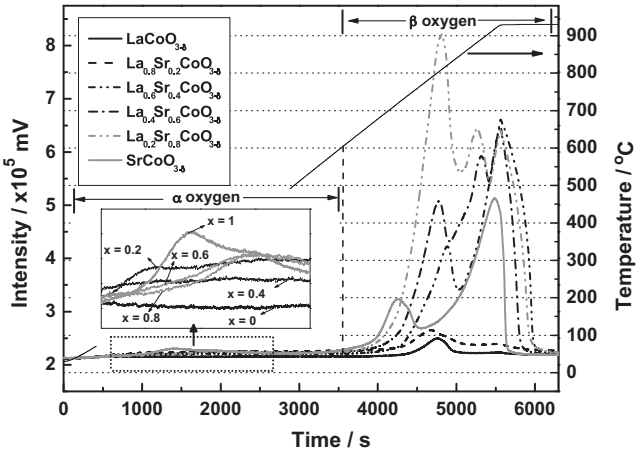

Fig. 5. O_2-TPD profiles for $La_{1-x}Sr_xCoO_{3-\delta}$ ($0 \le x \le 1$).

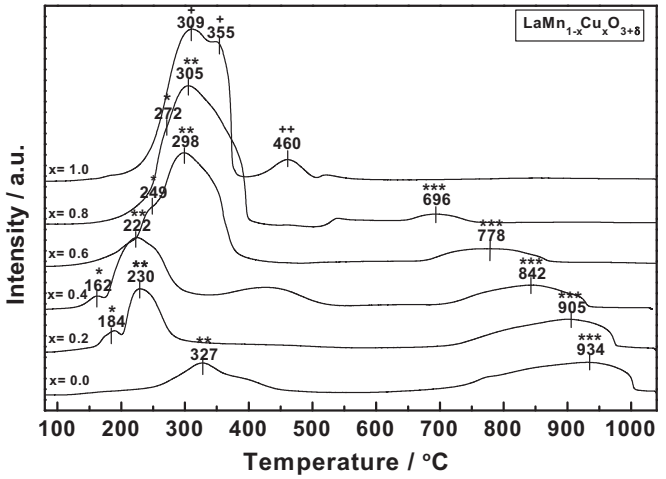

Fig. 6. TPR profiles for $LaMn_{1-x}Cu_xO_{3+\delta}$ ($0 \le x \le 1$): *: $Cu^{2+} \rightarrow Cu^{1+}$, **: $Cu^{1+} \rightarrow Cu^0$ and $Mn^{4+} \rightarrow Mn^{3+}$, ***: $Mn^{3+} \rightarrow Mn^{2+}$, +: reduction of CuO, and ++: reduction of Cu^{3+} in La_2CuO_4.

TPR tests were performed to investigate the reducibility of each perovskite catalyst. In this paper, we use the term 'reducibility' as a measure of how easily the substance is reduced by hydrogen, which is estimated based on the temperature at which the reduction begins. The TPR results are presented in Figs. 6 and 7 ($LaMn_{1-x}Cu_xO_{3+\delta}$) ($La_{1-x}Sr_xCoO_{3-\delta}$) with the assignation of TPR peaks based on the literature data [12,18,28–30]. In the TPR results for $LaMn_{1-x}Cu_xO_{3+\delta}$ (Fig. 6), copper was completely reduced from Cu^{2+} to Cu^0 (via Cu^{1+}), whereas the reduction of Mn^{4+} and Mn^{3+}terminated at Mn^{2+}[14,31]. The leading dual peaks were indicative of the reduction processes, $Cu^{2+} \rightarrow Cu^{1+}$

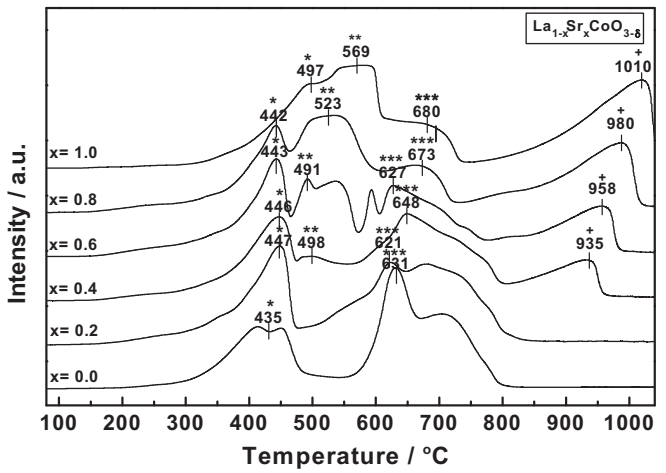

Fig. 7. TPR profiles for $La_{1-x}Sr_xCoO_{3-\delta}$ ($0 \le x \le 1$): *: $Co^{3+} \rightarrow Co^{2+}$, **: $Co_3O_4 \rightarrow CoO$, ***: $Co^{2+} \rightarrow Co^0$, and +: reduction of $SrCO_3$.

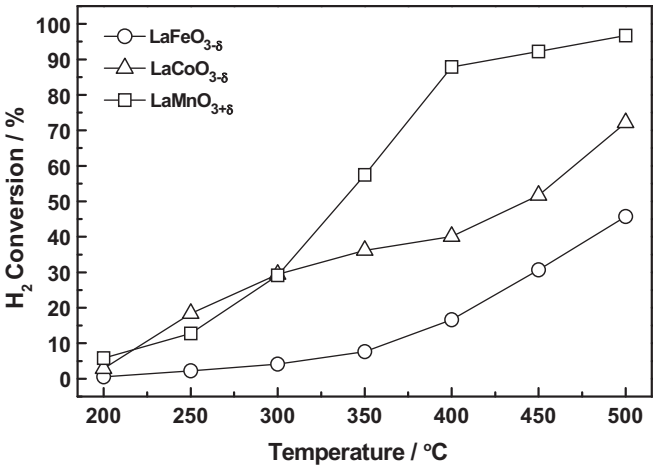

Fig. 8. Oxidation of hydrogen with non-substituted perovskites ($LaFeO_{3-\delta}$, $LaCoO_{3-\delta}$, $LaMnO_{3+\delta}$) under the simulated MCFC anode-off gas composition: 3.3% H_2, 10.7% O_2, 16.5% CO_2, 13.0% H_2O, N_2 balance; $w/f = 0.02\,g\,cm^{-3}$ s.

and $Mn^{4+} \rightarrow Mn^{3+}$ in sequence (the latter was overlapped by $Cu^{1+} \rightarrow Cu^0$), and the peak positions changed with the degree of Cu substitution (x): The $Mn^{4+} \rightarrow Mn^{3+}$ reduction in $LaMnO_{3+\delta}$ occurred at around 327 °C, but it shifted to 230 °C when x was 0.2 and then further to 222 °C at $x = 0.4$. The $Cu^{2+} \rightarrow Cu^{1+}$reduction also shifted to lower temperature as x was increased from 0.2 to 0.4, but then shifted higher as x was increased over 0.6. We were unable to confirm whether or not an x over 0.6 accompanied the shift of the $Mn^{4+} \rightarrow Mn^{3+}$ peak to a higher temperature from the precedent value (222 °C for $x = 0.4$), since the TPR peaks were undetectable. This was not only because Mn was greatly diluted at such high x values (x over 0.6), but also because the TPR intensity of Mn was inherently small compared to that of Cu. Therefore, in contrary to the literature [14], our TPR results could not be used to determine whether or not Mn^{4+} is stabilized upon incorporation of Cu^{2+}. However, the TPR results do reveal that Mn^{4+} and Cu^{2+} showed the greatest reducibility (i.e., the lowest reduction temperature) at Cu content (x) of 0.4.

In the TPR results of $La_{1-x}Sr_xCoO_{3-\delta}$ (Fig. 7), the reduction profiles of '*perovskitic*' Co^{+3} and Co^{+2}advanced that of $Co_3O_4$with regard to temperature. The Co_3O_4 and $SrCO_3$ peaks appeared from $x = 0.4$ and increased with further increment of x, which was in agreement with the XRD results (Fig. 2). The intensities of the reduction peaks for perovskitic, Co^{3+} and Co^{2+} were depressed with increment of Sr substitution, which was due to the presence of byproducts in the samples. The reduction temperature of perovskitic Co^{3+} ion was almost constant over the substitution degrees (x), leading to the conclusion that the reducibility of perovskitic Co^{+3} ion was not influenced by Sr^{2+} substitution. Hueso et al. previously presented similar results though XAS study [32].

3.2. Catalytic activities of $LaMn_{1-x}Cu_xO_{3+\delta}$ and $La_{1-x}Sr_xCoO_{3-\delta}$ for hydrogen combustion in a simulated MCFC anode off-gas

It is well known that the activity of a 'non-substituted,' single B-atom perovskite originates from the redox properties of B-site cations [33]. The H_2 conversions over non-substituted perovskites under simulated MCFC anode-off gas conditions are presented in Fig. 8. The order of activity was $LaMnO_{3+\delta} > LaCoO_{3-\delta} > LaFeO_{3-\delta}$.

As Mn of $LaMnO_{3+\delta}$ and La of $LaCoO_{3-\delta}$ were substituted by Cu and Sr respectively and the degree of each substitution increased, the total amount of removable oxygen, which was estimated as 'Total O-removed' in Table 1 from the TPR results, increased. However, this result was not directly correlated to the catalytic activities, since the TPR profiles contain the signals associated with the destruction of the perovskite structure, which is irrelevant at any rate to catalytic activity. We tried to find the major catalytic properties that govern the activities of $LaMn_{1-x}Cu_xO_{3+\delta}$ and $La_{1-x}Sr_xCoO_{3-\delta}$ for MCFC anode off-gas combustion.

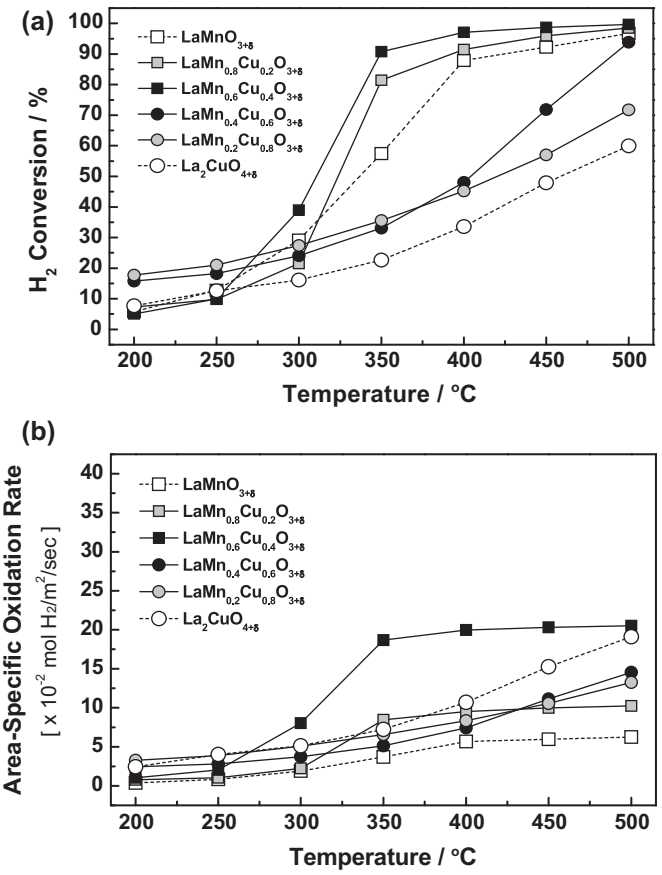

Fig. 9. Oxidation of hydrogen with $LaMn_{1-x}Cu_xO_{3+\delta}$ ($0 \le x \le 1$) under the simulated MCFC anode-off gas composition: (a) H_2 conversion and (b) *area-specific activity*: 3.3% H_2, 10.7% O_2, 16.5% CO_2, 13.0% H_2O, N_2 balance; $w/f = 0.02\,g\,cm^{-3}$ s.

The performance of $LaMn_{1-x}Cu_xO_{3+\delta}$ is presented in Fig. 9. The H_2 conversion profiles in Fig. 9a shows that the H_2 conversions over 300–450 °C were improved by increasing Cu substitution up to $x = 0.4$. With $LaMn_{0.6}Cu_{0.4}O_{3+\delta}$, the H_2 conversion exceeded 90% at 350 °C and approached 100% at 400 °C. However, further increase in Mn ($x = 0.6$ and 0.8) noticeably reduced H_2 conversion towards the level of the most inactive, Mn-less catalyst ($La_2CuO_{4+\delta}$). As already shown in Table 1 and Fig. 4, Cu substitution was accompanied by a decrease in specific surface area. The effect of surface area on catalytic activity was normalized by dividing the molar H_2 oxidation rate by the specific surface area, yielding an area-specific activity (Fig. 9b). Although the activity was re-evaluated in the area-specific standard, $LaMn_{0.4}Cu_{0.6}O_{3+\delta}$ and $LaMn_{0.2}Cu_{0.8}O_{3+\delta}$, remained inferior in performance, meaning that their low activities cannot be ascribed simply to their low surface areas. These two catalysts had the largest α-oxygen capacities among all $LaMn_{1-x}Cu_xO_{3+\delta}$ catalysts (in Table 1), so it was expected that the '*suprafacial* mechanism' by α-oxygen [10,17] would not be effective in the temperature range of 300–450 °C. Rather, the α-oxygen in these two catalysts seemed to have an effect at 200–250 °C where the catalysts showed slightly higher activities than the other catalysts having different substitution degrees (x). Meanwhile, $LaMn_{0.6}Cu_{0.4}O_{3+\delta}$ had an exceptionally high *area-specific activity* that was more than double those of other catalysts. It contained a modest amount

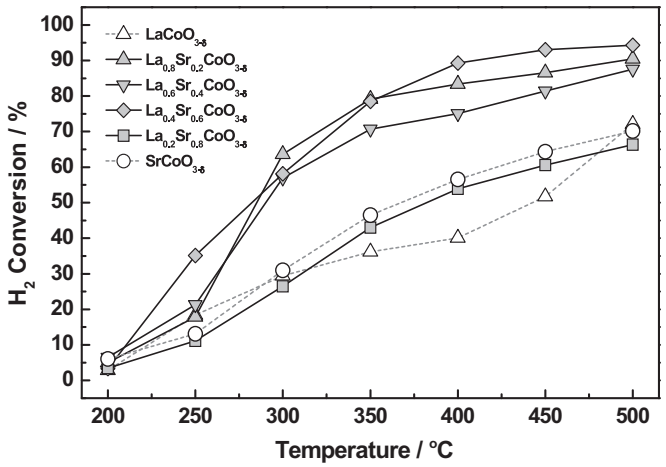

Fig. 10. Oxidation of hydrogen with $La_{1-x}Sr_xCoO_{3-\delta}$ ($0 \le x \le 1$) under the simulated MCFC anode-off gas composition: 3.3% H_2, 10.7% O_2, 16.5% CO_2, 13.0% H_2O, N_2 balance; $w/f = 0.02\ g\ cm^{-3}$ s.

of α-oxygen (Table 1) but as discussed before, its influence on the catalytic activity was expected to be minor. As such, its outstanding performance can most probably be attributed to the reducibility of Mn^{4+} and Cu^{2+} ions, which were estimated from the TPR tests. Meanwhile, $LaMn_{0.8}Cu_{0.2}O_{3+\delta}$, which was similar to $LaMn_{0.6}Cu_{0.4}O_{3+\delta}$ in the reducibility of Mn^{4+} and Cu^{2+}, did not show comparable *area-specific activity*. Another factor governing the activity of $LaMn_{1-x}Cu_xO_{3+\delta}$ is thought to be the mobility of oxygen. For the perovskite catalysts, active oxygen is thermally or chemically ejected from the surface and bulk of the material. The oxidative activity of a perovskite catalyst is firstly dependent on the amount (concentration) of active oxygen species, but in order to be effective, it should also be 'mobile' enough to migrate from the bulk to the surface. Chan et al. estimated that the oxygen mobility of $LaMn_{1-x}Cu_xO_{3+\delta}$ reached its peak at $x = 0.4$ with a value of two or four times higher than those of other catalysts at different x values [20]. This suggests that $LaMn_{0.6}Cu_{0.4}O_{3+\delta}$ surpasses $LaMn_{0.8}Cu_{0.2}O_{3+\delta}$ with regard to oxygen mobility, which was thus concluded to be the most probable cause of the significant difference in *area-specific activity* between the two catalysts.

The H_2 conversions with $La_{1-x}Sr_xCoO_{3-\delta}$ (Fig. 10) were initiated at a lower temperature than those with $LaMn_{1-x}Cu_xO_{3+\delta}$. As x was increased from 0.2 to 0.6, the H_2 conversion was increased to 50% at 300 °C. However, the H_2 conversions over 350 °C were inferior to those of $LaMn_{0.6}Cu_{0.4}O_{3+\delta}$. As clearly revealed in the figure, an increase in Sr substitution from $x = 0.2$ to 0.6 enhanced H_2 oxidation activity, which cannot be explained by the reducibility of cobalt cations, since, as discussed in the TPR results (Fig. 7), Sr substitution did not influence the reducibility of cobalt cations. Instead, Sr substitution promotes the generation of oxygen vacancies and influences the amount and reactivity of active oxygen species [15,17,20]. As reported in the literatures, the oxidative activity of $La_{1-x}Sr_xCoO_{3-\delta}$ usually reaches its maximum at $x = 0.2$ or 0.4, after which it drops monotonously with further Sr substitution [15,17,20]. Likewise, in Fig. 10, the catalysts at $x = 0.2$ and 0.4 were the most active. However, the catalyst at $x = 0.6$ was comparably active, which is contrary to the literature results. The unusually high activity of $La_{0.4}Sr_{0.6}CoO_{3-\delta}$ was attributed to a synergetic effect between perovskite and the by-produced Co_3O_4. As seen in the H_2-TPR results of Fig. 7, the reduction temperature of Co_3O_4 was close to that of perovskitic Co^{3+}, which implies the possibility of interaction between Co_3O_4 and the perovskite in the redox catalysis for H_2 oxidation. A similar theory of synergetic effect has been suggested in the literature. Simonot et al. showed that a mixture of $LaCoO_3$–Co_3O_4 is more active than $LaCoO_3$ alone in the oxidation of carbon monoxide [34]. The sole difference in our study is that Co_3O_4 mixed with $La_{1-x}Sr_xCoO_{3-\delta}$. Meanwhile, the activity dropped considerably when x was increased to 0.8, although the catalysts were composed of perovskite and Co_3O_4. This result implies that there exists an optimum range of mixture composition where the synergy is effective.

4. Conclusions

In a comparison of activities for the catalytic combustion of hydrogen in a simulated MCFC anode off-gas, $La_{1-x}Sr_xCoO_{3-\delta}$ was better than $LaMn_{1-x}Cu_xO_{3+\delta}$ in terms of initiation of activity, but the order was reversed for the level of full activity.

For $LaMn_{1-x}Cu_xO_{3+\delta}$, its activity was most strongly influenced by specific surface area, the reducibility of B-site metal cations and oxygen mobility. When normalizing the activity with specific surface area, the most active catalyst was $LaMn_{0.6}Cu_{0.4}O_{3+\delta}$, which was the most prominent in both B-site ion reducibility and oxygen mobility.

The $La_{1-x}Sr_xCoO_{3-\delta}$ prepared by the SGC method contained Co_3O_4 and $SrCO_3$ as by-products. The Co_3O_4 positively influenced the hydrogen combustion activity of the catalysts. Substitution of Sr^{2+} did not improve the reducibility of the perovskitic Co cations, but it did induce the generation of oxygen vacancies inside the catalyst. If these oxygen vacancies are considered the only source of activity, the activity should reach its peak at $x = 0.2$ or 0.4, as previously reported in many studies. However, the catalyst at $x = 0.6$ showed comparable activity, which could be attributed to the synergy in the redox mechanism between $La_{1-x}Sr_xCoO_{3-\delta}$ and by-produced Co_3O_4.

Acknowledgments

This work was supported by the National Research Foundation of Korea Grant funded by the Korean Government (MEST) (NRF-2009-C1AAA001-0093029).

Dr. Dae-Won Lee was supported by a Korea University grant.

All authors want to express their appreciation for the financial and experimental support provided by Doosan Heavy Industries & Construction Co. Ltd.

References

[1] K. Nath, D. Das, Curr. Sci. 85 (2003) 265–271.
[2] J. Zakzeski, P.C.A. Bruijnincx, A.L. Jongerius, B.M. Weckhuysen, Chem. Rev. 110 (2010) 3552–3599.
[3] M. Ditaranto, J.E. Hustad, T. Slungaard, A. Briand, Energy Fuels 21 (2007) 1982–1988.
[4] R. Prasad, L.A. Kennedy, E. Ruckenstein, Catal. Rev. Sci. Eng. 26 (1984) 1–58.
[5] J. Kirchnerova, Korean J. Chem. Eng. 16 (1999) 427–433.
[6] R.J.H. Voorhooeve, D.W. Johnson Jr., J.P. Remeika, P.K. Gallagher, Science 195 (1977) 827–833.
[7] H. Tanaka, M. Misono, Curr. Opin. Solid State Mater. Sci. 5 (2001) 381–387.
[8] T.V. Choudhary, S. Benerjee, V.R. Choudhary, Appl. Catal. A: Gen. 234 (2002) 1–23.
[9] A.S. Bhalla, R. Guo, R. Roy, Mater. Res. Innovations 4 (1999) 3–26.
[10] D. Fino, N. Russo, G. Saracco, V. Specchia, J. Catal. 217 (2003) 367–375.
[11] H. Arai, T. Yamada, K. Eguchi, T. Seiyama, Appl. Catal. 26 (1986) 265–276.
[12] J.G. McCarty, H. Wise, Catal. Today 8 (1990) 231–248.
[13] Z.B. Chen, T.R. Ling, M.-D. Lee, React. Kinet. Catal. Lett. 62 (1997) 185–190.
[14] L. Lisi, G. Bagnasco, P. Ciambelli, S. De Rossi, P. Porta, G. Russo, M. Turco, J. Solid State Chem. 146 (1999) 176–183.
[15] N. Yamazoe, Y. Teraoka, Catal. Today 8 (1990) 175–199.
[16] J. Niu, J. Deng, W. Liu, L. Zhang, G. Wang, H. Dai, H. He, X. Zi, Catal. Today 126 (2007) 420–429.
[17] T. Seiyama, Catal. Rev. Sci. Eng. 34 (1992) 281–300.
[18] F.C. Buciuman, F. Patcas, J.C. Menezo, J. Barbier, T. Hahn, H.-G.T. Lintz, Appl. Catal. B: Environ. 35 (2002) 175–183.
[19] X. Yang, D.W. Park, M.I. Kim, Korean J. Chem. Eng. 24 (2007) 592–595.
[20] K.S. Chan, J. Ma, S. Jaenicke, G.K. Chuah, Appl. Catal. A: Gen. 107 (1994) 201–227.

[21] H. Yasuda, N. Mizuno, M. Misono, J. Chem. Soc., Faraday Trans. 90 (1994) 1183–1189.
[22] C.K. Rhee, H.I. Lee, Korean J. Chem. Eng. 11 (1994) 48–54.
[23] B. He, Q. Song, Q. Yao, Z. Meng, C. Chen, Korean J. Chem. Eng. 24 (2007) 503–507.
[24] C. Tofan, D. Klvana, J. Kirchnerova, Appl. Catal. B: Environ. 36 (2002) 311–323.
[25] Z. Gaoke, L. Ying, Y. Xia, W. Yanping, O. Shixi, L. Hangxing, Mater. Chem. Phys. 99 (2006) 88–95.
[26] R.J.H. Voorhoeve, J.P. Remeika, L.E. Trimble, Ann. N. Y. Acad. Sci. 272 (1976) 3–21.
[27] J. Zhua, Z. Zhao, D. Xiao, J. Li, X. Yang, Y. Wu, J. Mol. Catal. A: Chem. 238 (2005) 35–40.
[28] F. Buciuman, F. Patcas, J. Zsakó, J. Therm. Anal. Calorim. 61 (2000) 819–825.
[29] L. Huang, M. Bassir, S. Kaliaguine, Appl. Surf. Sci. 243 (2005) 360–375.
[30] J.P. Dacquin, C. Dujardin, P. Granger, J. Catal. 253 (2008) 37–49.
[31] M.L. Rojas, J.L.G. Fierro, L.G. Tejuca, A.T. Bell, J. Catal. 124 (1990) 41–51.
[32] J.L. Hueso, J.P. Holgado, R. Peregñíuenz, S. Mun, M. Salmeron, A. Caballero, J. Solid State Chem. 183 (2010) 27–32.
[33] Y.I. Pyatnitsky, N.I. Ilchenko, L.Y. Dolgikh, N.V. Pavlenko, Top. Catal. 11–12 (2000) 229–237.
[34] L. Simonot, F. Garin, G. Maire, Appl. Catal. B: Environ. 11 (1997) 167–179.